scientific reports

OPEN

Detection of probable phytochemical inhibitors targeting kallikrein related peptidase 7 (KLK7) in ovarian cancer through molecular dynamics and virtual screening approaches

Ameena Farooq[1], Rana Muhammad Mateen[1], Muhammad Ali[1], Mohsin Javed[2], Ayed A. Dera[3], Ahmad Asimov[4], Syed Kashif Ali[5,6], Fadi Jaber[7,8], Safura Bibi[9], Ali Bahadur[10,11✉], Shahid Iqbal[12✉], Sajid Mahmood[13,14], Randa A. Althobiti[15] & Abeer Ahmed Alghamdi[16]

High-grade serous ovarian carcinoma (HGSOC) is the predominant and most lethal form of ovarian cancer, originating from the epithelium of the fallopian tubes. It has been shown that HGSOC subtype II epithelial ovarian cancer accounts for 50–70% of all ovarian malignancies. It is the most common cause of mortality for women with ovarian cancer. By using in-silico techniques to find out potential drugs against his disease, this study seeks to report the need for efficient treatments. The protein kallikrein-related peptidase 7 (KLK7), whose overexpression leads to HGSOC, was chosen as a drug target. Based on their Absorption, Distribution, Metabolism, Excretion, and Toxicity (ADMET) characteristics, the ligands were carefully picked from the IMPATT library that contained 17,967 phytochemicals. Auto Dock Vina was then used to dock the 88 finalized compounds against the protein. Density Functional Theory (DFT) and molecular dynamic simulation analyses were used to assess the compound that was the most stable with the protein. The protein-ligand combination was stable during the MD simulation. Post simulation analysis, such as RMSF (Root Mean Square Deviation), RMSD (Root Mean Square Deviation), Rg (Radius of Gyration), and HB (Hydrogen Bonding), revealed the stability of the proposed compound with the KLK7 protein.

[1]Department of Life Sciences, School of Science, University of Management and Technology (UMT), Lahore 54770, Pakistan. [2]Department of Chemistry, School of Science, University of Management and Technology, Lahore 54770, Pakistan. [3]Department of Clinical Laboratory Sciences, College of Applied Medical Sciences, King Khalid University, Abha, Saudi Arabia. [4]Composite Materials Scientific Research Center of Azerbaijan State University of Economics, 194 Murtuza Mukhtarov, AZ1065 Baku, Azerbaijan. [5]Department of Physical Sciences, Chemistry Division, College of Science, Jazan University, P.O. Box. 114, 45142 Jazan, Kingdom of Saudi Arabia. [6]Nanotechnology Research Unit, Jazan University, P.O. Box. 114, 45142 Jazan, Kingdom of Saudi Arabia. [7]Department of Biomedical Engineering, Ajman University, Ajman, UAE. [8]Center of Medical and Bio-Allied Health Sciences Research, Ajman University, Ajman, UAE. [9]Department of Botany, University of Agriculture, Faisalabad 38040, Pakistan. [10]Nanomaterials Research Center, Department of Chemistry, College of Science, Mathematics, and Technology, Wenzhou-Kean University, Wenzhou 325060, Zhejiang Province, China. [11]Dorothy and George Hennings College of Science, Mathematics and Technology, Kean University, 1000 Morris Ave, Union, NJ 07083, USA. [12]Nottingham Ningbo China Beacons of Excellence Research and Innovation Institute, University of Nottingham Ningbo China, Ningbo 315100, China. [13]Low Dimensional Materials Research Center at, Khazar University, AZ1096 Baku, Azerbaijan. [14]Faculty of Science and Technology, ILMA University, Karachi, Pakistan. [15]Department of Chemistry, College of Science, University of Bisha, P.O Box 551, 61922 Bisha, Saudi Arabia. [16]Department of Physics, College of Science, Princess Nourah bint Abdulrahman University, P.O. Box 84428, 11671 Riyadh, Saudi Arabia. ✉email: abahadur@wku.edu.cn; shahidgcs10@yahoo.com

Although it is uncommon, ovarian cancer is the most fatal form of reproductive cancer and a significant national health problem. The ovarian external epithelium can develop malignant changes that lead to epithelial ovarian cancer[1]. Epithelial ovarian cancer has been divided into type I and type II ovarian carcinomas based upon recent categorization[2]. High-grade serous carcinoma (HGSC) is the most widespread kind of epithelial ovarian cancer, belonging to type II. The most common cause of ovarian cancer mortality is HGSC subtype II epithelial ovarian cancer[3]. When it comes to novel HGS carcinoma, cytoreductive surgery, also known as debulking surgery, is often the first therapy option[4]. The disease progression is monitored by platinum-based chemotherapy[5].

The most prevalent and deadly kind of ovarian cancer is HGSOC. Chromosome abnormalities, gene changes such as TP53 (a gene that helps prevent cancer), DNA damage, oxidative stress from hazardous substances in the body, and a high requirement for energy in the cells are some of the key features[6–9] This increased energy demand makes it harder for the cells to deal with damaged or unwell shaped proteins. It has been found that the assembly between the Fallopian tube and HGSC is reinforced when comparable TP53 mutations were found in fallopian tube malignancies. Mutations in the TP53 gene are found in almost all cases of HGSC[10–12]. A significant problem is genetic volatility, as DNA during malignancy is always changing. Clinical reactions to drugs that mark abnormalities in HRR in BRCA1/2, as well as gene expression readings of germline BRCA1/2 mutant and wild-type cancers, also contribute to high-grade serous carcinoma[13].

The protein kallikrein-related peptidase 7 (KLK7) is a potential target for therapeutics. This protein is overexpressed in HGSC. The KLK family comprises 15 closely related serine proteases and is situated on the long arm of chromosome 19q13.4. KLK7, a chymotrypsin-like serine protease within the KLK family, cleaves after phenylalanine, tyrosine, and leucine[14]. According to recent research, elevated KLK7 protein levels have an impact on HGSOC prognosis. According to research on KLK7's possible role in HGSOC, it promotes α5/β1 integrin-dependent cell adhesion and multicellular aggregates (MCA), both of which increase peritoneal proliferation and reinvasion. As a result, this promotes paclitaxel resistance, metastasis, and invasion of ovarian cancer cells. KLK7 may facilitate tumor cell invasion and metastasis by cleaving extracellular matrix (ECM) proteins and other adhesion molecules such as desmoglein-1 and desmocollin-1. Through the activation of matrix metalloproteinase-9 (MMP-9), KLK7 has been shown to be crucial for tumor cell motility, invasion, and angiogenesis in carcinomas. This suggests that KLK7 also contributes to the formation of tumors[15].

While KLK7 has been implicated in promoting tumor progression, metastasis, and chemoresistance in HGSOC, there are currently no KLK7 inhibitors approved for clinical use. A few synthetic inhibitors and peptide-based compounds have been investigated in the past; however, many of these suffer from limitations such as poor selectivity, low metabolic stability, and reduced bioavailability[15]. These challenges underscore the need for alternative scaffolds with improved drug-like properties. Our study aims to fill this gap by identifying phytochemical candidates, specifically *Aristolactam-N-β-D-glycoside,* as potential KLK7 inhibitors using an in silico approach. This not only introduces structural novelty but also explores the untapped potential of natural compounds in targeting KLK7.

Methodology
Protein 3D structure selection and verification
The prime cause of high-grade serous ovarian cancer is protein overexpression. Mostly, the overexpressed protein that contributes to the development of HGSOC was chosen. KLK7 is one of these proteins. Furthermore, the protein's structure was confirmed.

Structural selection
The HGSOC kLK7 protein structure was selected from PDB, and it has PDB ID: 6Y4S https://doi.org/10.2210/pdb6Y4S/pdb. Its resolution is 2.23 Å, and its structure has 224 amino acids. According to a recent study, amplified KLK7 protein levels affect the prognosis of HGSOC. According to studies on KLK7's probable involvement in HGSOC, it stimulates α5/β1 integrin-dependent cell adhesion and multicellular aggregates (MCA), which in turn encourage ovarian cancer cell invasion, metastasis, and paclitaxel resistance[15]. The next stage is to authenticate the structure of the chosen protein using a variety of tools, such as ERRAT, PRO CHECK, and VERIFY 3D. The protein should first be purified, meaning that any unnecessary chains should be cut out. Software called Discovery Studio Visualizer 21.1.0.20298 was used to bring out this purifying procedure.

Structure verification
Authentication of the 3D structure of KLK7 was done using numerous tools that include ERRAT https://www.doe-mbi.ucla.edu/errat[16], PRO CHECK https://www.ebi.ac.uk/thornton-srv/software/PROCHECK/[17], as well as VERIFY 3D https://www.doe-mbi.ucla.edu/verify3d[18]. The results advocated that the protein was of good quality. Structural validation was done to guarantee the structural reliability of the protein.

Active site prediction
Since the medication will be prepared for those target site amino acids, one of the most critical steps was predicting the protein's active site. First, every protein's target site was observed in literature reviews. Only a few amino acids are mentioned in the literature in various protein research. Then, after widespread searching, three different tools were used for the estimate of the target site that includes, including COACH https://zhanggroup.org/COACH/[19], Castp http://sts.bioe.uic.edu/castp/index.html?2pk9[20] and Prankweb https://prankweb.cz/[21]. These are the tools that primarily estimate which certain amino acids will be present at the target location.

Following that, the entire protein result from the literature and these tools were associated. The predicted amino acid sequences found in the protein's active sites were used to choose the results from at least three websites.

Preparation of receptor and ligand for molecular docking

Preparation of receptor

Using BIOVIA Discovery Studio Visualizer, the protein KLK7 was first filtered to remove any non-protein entities, ligands, heteroatoms, and matching water molecules. Continue eliminating all additional entities from the 224 amino acid residues of the KLK7 protein chain A. Following purification, AutoDock tools v 1.5.7 were used to further store both proteins in PDB format[22] and receptor preparation was done, transforming the PDB format to pdbqt format.

Ligand library

The ligand library was occupied from Indian Medicinal Plants, Phytochemistry and Therapeutics 2.0 (IMPPAT 2.0), which is an online library of phytochemicals (https://cb.imsc.res.in/imppat/).

Screening of ligand library

A total of 17967 ligands were extracted from the IMPPAT 2.0 library and filtered using the ADMET criteria given in Table 1. The 17967 compound library was subjected to Lipinski and colleagues' rule of five in order to ascertain the compounds' drug likelihood[23]. The Veber rule (number of rotatable bonds ¼ fewer than 10 and total polar surface area ¼ less than 140) was then used to assess the oral practicality of medications[24]. The MCDK (more or equal to 30) criteria were dropped in favor of a more thorough investigation of the toxicity and efficacy of water solubility. Additional screening was carried out by the Veber rule and the fifth Lipinski rule to ascertain the compounds' cardiotoxicity (hERG pIC50 less than 5.5 and hERG Filter ¼ No) and carcinogenicity (BCRP inhibitor TD50 more than 25). Table 1 shows the selection criteria utilized for 17967 compounds.

Ligand preparation

The ligands were taken from the IMPPAT library. Biovia Discovery Studio translated these ligands from SDF format to PDB configuration after downloading them. The ligand was further altered to pdbqt format using AutoDock vina v1.5.7 by adding hydrogen and Kollman charges[25].

Grid box generation

This critical stage of the HGSOC drug design process includes building grid boxes with AutoDock Vina for more molecular docking simulations. In essence, this phase creates the search space in which the ligands will interrelate with the site of our choice. Since this confirms the comprehensive analysis of the conformational space throughout the docking process, we first set the exhaustiveness value for the protein to 8. The structural characteristics and functional importance of each domain were used to determine additional grid box criteria, such as grid size and center coordinates. To enable the following processing steps, the completed grid box configurations were stored in each domain configuration file. Specific amino acids within each domain were initially recognized, and any extraneous residues were removed to produce properly specified active sites.

Following the addition of polar hydrogen bonds, Kollmann charges were used at each active site to improve precision. Autodock Vina is used to create a grid for the protein. The grid considerations for each domain were suitably modified, and the size of the grid box was chosen to guarantee exhaustiveness and spacing. To enhance molecular docking research, proteins' active site KLK7 was discovered and employed as a grid preparation centre. AutoDock 1.5.7v tools[22] were used to produce grids around these active site residues. The specific parameters for the protein are as follows: The active site residues for KLK7 include SER195, HIS57, ASN189, TRP215, GLY216, and PHE218. The grid was positioned at − 41.251 Å, 16.146 Å, and 29.463 Å, with dimensions measuring 38 in the x direction, 32 in the y direction, and 34in the z direction. The exhaustiveness parameter was configured to 8 for this docking setup.

No. of properties	ADMET properties	Recommended ranges
1	Lipinski's rule of five (ROF)	≤ 5
	HBA	< 500 Dalton
	Molecular weight	≤ 10
	HBD	≤ 5
	Log P	
2	Water solubility (Sw)	≥ 0.010 mg/mL
3	Apparent Madin-Darby canine kidney cell permeability (MDCK)	≥ 30 cm/s × 10^7
4	Log BB	< − 1 (for BBB-)
5	Blood–Brain Barrier filter	Low (%) (for BBB-)
6	BCRP_Inh	No
7	hERG filter	No
8	hERG pIC50	< 5.5
9	Skin sensitivity (sensitizer)	No

Table 1. Criteria selected for library preparation for molecular docking.

Molecular docking

Following the definition of the protein's grid box and the meticulous acquisition of our FDA-approved ligand library, we proceeded to the subsequent stage of the procedure, known as molecular docking. Auto Dock Vina was utilized to dock 88 compounds with protein KLK7 receptors. The collaboration between the ligand and receptor was assessed using the BIOVIA Discovery Studio Visualizer. We had to establish our data files into sets, which contained Vina setup files (Downloads—AutoDock Vina, Setup files), configuration files with the grid box results, and error-free receptor and ligand files, to begin the docking process. The docking requires the files that were retrieved. The docking process is executed using the vina-config conf. txtlog log.txt command. By pointing to the configuration file and log.txt file, this program started the Auto Dock Vina. While the log. txt file held the binding affinities and estimated ligand posture coordinates required for the docking procedure, the configuration file contained the exact grid box settings. Therefore, molecular docking between the ligands, which were taken from IMPPAT, and the protein KLK7 as a receptor was done.

Density functional theory

The DFT is used to ascertain the ligand's level of reactivity. The ten ligands using the lowest binding energies were investigated for DFT analysis. An energy gap known as the delta-E splits the Lowest Unoccupied Molecular Orbital (LUMO) from the Highest Occupied Molecular Orbital (HOMO)[26]. The DFT analysis was performed using Gaussian 09, and the recovered file fragment format of the chk file was shown using GaussView 6.0.

Molecular dynamics simulation

To understand the protein–ligand interaction, it is critical to comprehend the molecular dynamics between the protein and the ligand. In this case, the protein is the KLK7, whereas the ligands were taken from IMPPAT. For this purpose, the molecular dynamics simulations were conducted[27]. The top ten docked complexes with the highest negative energies underwent NAMD, or nanoscale molecular dynamics. It utilizes CHARMM++ and VMD, which stands for Visual Molecular Dynamics[28] for visualisation. The MD simulation proceeded for 100 ns. For analysis through VMD of the RMSD, Rg, hydrogen bonds, and RMSF were done, which generated results as graphs.

Results and discussion

2Structure validation of protein

The protein structure with ID 6y4s was retrieved from PDB, and its 3D structure was validated through ERRAT[29], Verify3D[30] plans of an online server called Structure Analysis and Verification Server version 6 (*SAVES* v6.0). The Ramachandran plot of PROCHECK for KLK7, 99.5% of the residues were present in the allowed region. The 3D structure of the protein obtained from PDB is shown in Fig. 1.

Screened ligands

From the library of 17,967 phytochemicals, 4899 compounds were screened after applying Lipinski's rule of five and further applying water solubility, MCDK, log BB, BBB filter, BCRP, hERG filter, and hERG pIC50 total of 88 ligands were screened (Scheme 1). The criteria for the hERG filter were set to NO to ensure that the screened compounds do not bind to the potassium channels encoded by the hERG gene, as this can lead to fatal ventricular arrhythmias and sudden death. The screened 88 compounds were ultimately docked at the active sites of the protein KLK7. Since this cancer is not found in the brain, a total of 88 compounds were in the negative blood–brain barrier group. The number of screened ligands across all parameters can be seen in Table 2.
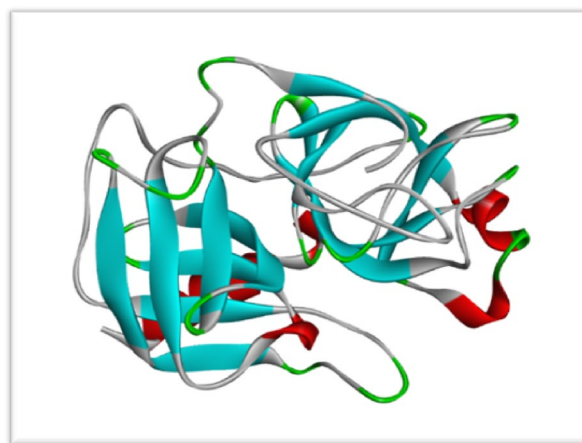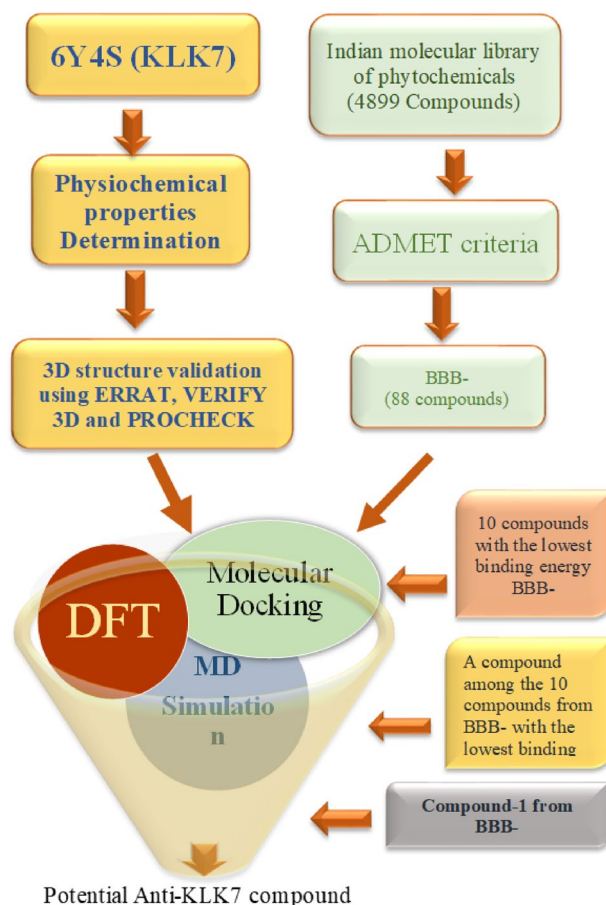

Fig. 1. 3D structure of protein kallikrein-related peptidase 7 (KLK7) (PDB ID: 6Y4S, Resolution: 2.23 Å, Chain A) human protein. (It was drawn using the software Discovery Studio Visualizer (2021 version).

Scheme 1. Overview of screening of potential inhibitors for protein KLK7 overexpressed in HGSOC.

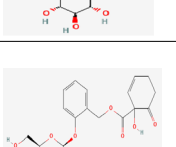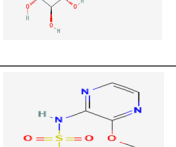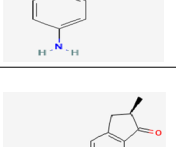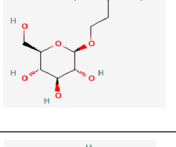| Sr. No	ADMET criteria	Recommended ranges	Screened ligands
1	Water solubility (Sw)	≥0.010 mg/mL	4899
2	Apparent Madin-Darby canine kidney cell permeability (MDCK)	≥30 cm/s×10^7	4078
3	Log BB	<−1 (for BBB-)	165
4	Blood–Brain Barrier filter	Low (%) (for BBB-)	112
5	BCRP_Inh	No	102
6	hERG Filter	No	100
7	hERG pIC50	<5.5	88
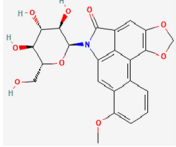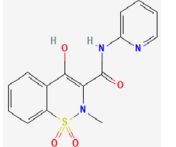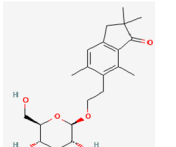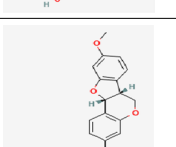
Table 2. Ligands were screened according to ADMET criteria from the IMPPAT library of phytochemicals. No. of ligands screened, blood brain barrier negative group = 88.

Docking analysis

A total of eighty-eight compounds were docked at the active sites of the respective protein (KLK7) to inhibit the protein. The top ten ligands with their lowest binding energies, IUPAC names, PubChem ID, structure, molecular formula, and interacting residues are shown in Table 3. For KLK7, the lowest energies were −8.2 kcal/mol to −7.2 kcal/mol. To visualize and analyse the connections between the ligand and the receptor, BIOVIA Discovery Studio Visualizer was utilized.

Docking analysis of KLK7

Out of all the lowest binding energy compounds for KLK7, compound no. 1,14-methoxy-10-[(2S,3R,4S,5S,6R)-3,4,5-trihydroxy-6-(hydroxymethyl)oxan-2-yl]-3,5-dioxa-10   azapentacyclo[9.7.1.02,6.08,19.013,18]nonadeca-1(18),2(6),7,11(19),12,14,16-heptaen-9-one (Aristolactam-N-beta-D-glycoside) with PubChem ID 159819 had the lowest binding energy of −8.2 kcal/mol. BIOVIA Discovery Studio Visualizer was applied to visualize the interactions and the results between the ligand and the receptor. The interaction between compound 1 and the ligand includes Van der Waals forces shown between CYS220, PHE218, THR217, TYR172, and THR98. Conventional Hydrogen bond between ASN192, GLY216, Pi-Cation bond between TRP215, HIS99, and Pi-

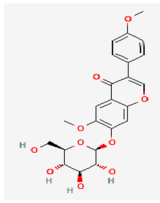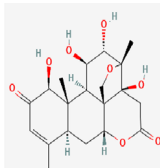| Sr no	Common name	BE Kcal/mol	Structure	MF	HB	VDW	Others
1	Aristolactam-N-beta-D-glycoside	− 8.2		$C_{23}H_1NO_9$	ASN192, GLY216	CYS220, PHE218, THR217, TYR172, THR98	LEU175
2	Piroxicam	− 8.0		$C_{15}H_{13}N_3O_4S$	CYS220, GLY216, ASN192, HIS57, SER195	VAL213, SER214, CYS191, THR217, PHE218	TRP215, ALA190, CYS42
3	Pteroside z	− 7.8		• $C_{21}H_{30}O_7$	CYS220, SER214, HIS57, SER195	LEU175, THR98, HIS99, ALA190, CYS191, VAL213, PHE218, THR217	TRP214, GLY216, ASN192
4	Medicarpin glucoside	− 7.7		$C_{22}H_{24}O_9$	HIS99, GLN97, THR96	ASN192, THR217, SYS191, GLY216, VAL227, SER214, SER195, THR98	ASN189, TRP215, GLY216, HIS57, ALA190, VAL213, CYS220
5	Salicortin	− 7.6		• $C_{20}H_{24}O_{10}$	GLY193, ASN192, SER195, THR217	HIS99, TRP215, PHE218, CYS22, GLY216 CYS191, SER214, VAL213, ALA190	HIS41, CYS42
6	4-amino-N-(3-methoxypyrazin-2-yl)benzenesulfonamide	− 7.5		$C_{11}H_{12}N_4O_3S$	His57, SER195, ASN189, GLY216, SER214	ASP194, VAL213, GLy220, PRO225, GLY226, ASN192	CYS220, ALA190
7	Sulfalene	− 7.5		$C_{20}H_{28}O_7$	SER195, ALA190	LEU175, HIS57, HIS99, ASP194, ASN192, SER214, VAL213, CYS191, ASN189, CYS220, PHE218	TRP215 GLY216 THR217
8	Boeravinone B	− 7.4		• $C_{17}H_{12}O_6$	SER195, THR217	HIS57, SER214, VAL213, TRP215, ALA190, CYS191, CYS220, ASN192, PHE218	GLY216
Continued							

Sr no	Common name	BE Kcal/mol	Structure	MF	HB	VDW	Others
9	Wistin	− 7.2		$C_{23}H_{24}O_{10}$	GLY193, THR217	SER35, GLN39, HIS41, LEU40, ASN192, VAL213, TRP215, PHE218, VAL227, ALA190, CYS191, CYS220, GLY216	SER195, HIS57
10	Samaderine E	− 7.2		$C_{20}H_{26}O_{8}$	ASN192	LEU175, THR217, PHE218, TRP215, GLY216, HIS99, HIS57, SER195	SER214

Table 3. The top 10 compounds with their binding energies (BE), structural information, and interacting residues of the KLK7 protein with the docked ligands from the IMPATT library are shown below BE, binding energy; MF, molecular formula; HB, hydrogen-bonds; VDW, Van der Waals; MF, molecular formula.

Alkyl bond between LEU 175 were seen as shown in Fig. 2. HIS99 makes two bonds; one pi-alkyl bond with a distance of 5.23 Å and one pi-cation bond with a distance of 5.13 Å. TRP215 also makes two pi-cation bonds with the aromatic rings of the ligands, with the distance of 5.78 Å and 4.41 Å, and LEU175 makes a pi-alkyl bond with the distance of 5.00 Å. Conventional hydrogen bond interaction exists between the ligand and ASN 192 and GLY 216, the distance is 2.10 Å and 2.70 Å.

The abovementioned ligand structures were taken from the PubChem database and have been verified.

Reference compound analysis
Docking analysis
Receptor protein KLK7 was docked with the Reference compound (Aristolactam-N-beta-D-glycoside), with PubChem ID 159819 had a binding energy of − 8.2 kcal/mol. BIOVIA Discovery Studio Visualizer was utilized to visualize the interactions and the results between the ligand and the receptor. The interaction between compound 1 and ligand includes Van der Waals forces shown between CYS220, PHE218, THR217, TYR172, and THR98. Conventional Hydrogen bond between ASN192, GLY216, Pi-Cation bond between TRP215, HIS99, and Pi-Alkyl bond between LEU 175 were seen as shown in Fig. 2 and Figures S1-S10. HIS99 makes two bonds; one pi-alkyl bond with a distance of 5.23 Å and one pi-cation bond with a distance of 5.13 Å. TRP215 also makes two pi-cation bonds with the aromatic rings of the ligands, with a distance of 5.78 Å and 4.41 Å, and LEU175 makes a pi-alkyl bond with a distance of 5.00 Å. Conventional hydrogen bond interaction exists between the ligand and ASN 192 and GLY 216, the distance is 2.10 Å and 2.70 Å.

DFT analysis
Gaussview 6.0 is used to visualize DFT results, and the energy gap (ΔE), which is determined by the difference between E$HOMO$ and E$LUMO$, was computed for each of the ten ligands that were chosen during docking (Table 4). Compound-1 has the lowest binding energy of any ligand, with a ΔE of 0.13272 eV. The molecule is reactive because of the small energy gap (Fig. 3).

Molecular dynamics simulation
An MD simulation of KLK7 was run for 100 ns using NAMD 2.14[27] software, and the outcomes were examined for RMSD, Rg, hydrogen bond formation, RMSF, and hydrogen bond trajectory using VMD[28]. The RMSD[31] illustrates the stability of the protein, ligand, and protein–ligand complex. It states that the Rg[32] is the parameter for 3D structural compactness. The RMSF[31] method is used to calculate the variation of amino acid residues. It demonstrates how protein–ligand complexes have a structure–function link.

KLK7 analysis of molecular dynamic simulation
RMSD analysis   Root mean square deviation (RMSD) indicates stability for the KLK7 and Aristolactam-N-beta-D-glycoside complex. During MD simulation analysis, RMSD displays the stability of the protein, ligand, and protein–ligand complex. There should be no more than 5 Å in the RMSD number. Throughout 120 ns, the KLK7 and Aristolactam-N-beta-D-glycoside combination exhibited stability with a fluctuation of about 2.8 Å. There is a 2 Å fluctuation in the protein. There should be no more than 5 Å in the RMSD number.

RMSF analysis   The KLK7 protein residues vary during the MD simulations, as seen by the RMSF plot in Fig. 4D. The variation of the protein KLK7 residues is displayed in the first and last 1000 frames. The protein is

(A)

(B)   (C)

Fig. 2. Detailed view of the docked complex of the KLK7 protein with the top ligand, Aristolactam-N-beta-D-glycoside. (**A**) Binding pose of Aristolactam-N-beta-D-glycoside in the active site pocket of KLK7 protein with a zoomed-out view and a zoomed-in square shape picture showing a closer view on the right side. (**B**) Two-dimensional map depicting residues along with their specific bonding. (**C**) Illustrates the H-bond interactions of residues. (**D**) Mode of interactions in 3D representation. (It was drawn using the software Discovery Studio Visualizer (2021 version).

stable throughout the MD simulation system, as evidenced by the fluctuations in the residues in the first and last sections. The range of the RMSF values is nearly 0.7 to 2 Å. This specifies that the protein residues are steady because the fluctuation is within the threshold range. There is little variation in the active site amino acids. This suggests that the residues of the active site amino acids exhibit stability during the MD Simulation.

Radius of gyration   The protein's compactness is indicated by the Radius of Gyration during MD simulation. Under a radius of gyration value of about 23 Å, the protein KLK7 exhibits stable density, which is regarded as being within a good range. Thus, as the radius of gyration graph in Fig. 4 illustrates, the protein structure stayed compact and stable during MD simulation analysis.

Hydrogen bonds   The percentage of hydrogen bonding is also examined using the Molecular Dynamics (MD) simulation. Water molecules, ligands, and ions envelop the protein–ligand complex. The hydrogen bonds, which are in charge of the protein–ligand complex's stability and selectivity, demonstrate the protein's stability. The

Sr No	Pubchem ID	Dipole moment (Debye)	HOMO (eV)	LUMO (eV)	Band energy gap ΔE (eV)
1	159819	7.150077	− 0.19569	− 0.06297	0.13272
2	54676228	4.861522	− 0.23816	− 0.08813	0.15003
3	169737	5.786751	− 0.23466	− 0.05191	0.18275
4	23724664	3.153959	− 0.20431	− 0.00985	0.19446
5	115158	2.132715	− 0.25536	− 0.04767	0.20769
6	134379	5.277355	− 0.22872	− 0.05144	0.17728
7	9047	9.083936	− 0.22391	− 0.05918	0.16473
8	14018348	2.878331	− 0.21788	− 0.07515	0.14273
9	10095770	2.032525	− 0.22178	− 0.06558	0.1562
10	10475714	4.687391	− 0.25429	− 0.07187	0.046441

Table 4. DFT analysis of ten selected compounds with the lowest binding energy of KLK7. HOMO, Highest occupied molecular orbital; LUMO, Lowest unoccupied molecular orbital.

quantity of hydrogen bonds created shows that the protein is consistently attached and powerfully attracted, as seen in Fig. 4.

Discussion

Ovarian cancer is the greatest incurable form of reproductive malignancy and a major public health issue[33]. The ovarian surface epithelium, which is next to the peritoneal epithelium, can develop malignant changes that lead to epithelial ovarian cancer[34]. Recent improvements in histology, molecular and genetic research, and classification have led to the classification of epithelial ovarian cancer into type I and type II ovarian carcinomas[35]. A class of neoplasms that originate from germinal tissues and have unique clinical, pathological, and molecular features is referred to as ovarian malignancies. With five different tumor isotypes, epithelial ovarian malignancies (EOCs) are the most common of them. Notably, more than 70% of EOC cases are HGSOCs, which make up the majority[36]. HGSOC is still challenging to treat. Although endogenous immunity at the molecular or T cell level may make immunotherapy for HGSOC responsive, it has not yet fulfilled its potential[37]. Nearly 300,000 women were diagnosed with ovarian cancer in 2018; the International Federation of Gynecology and Obstetrics categorized the majority of these cases as stage III/IV[38]. The usual first-line treatment for advanced HGS carcinoma is a cytoreductive (debulking) surgical procedure monitored by platinum and paclitaxel-based chemotherapy. Although the majority of patients endure chronic disease three years after beginning initial medication, about 70% of women have an extraordinary initial response to treatment[39].

Some studies have focused on hormonal balance through natural compounds[40]. Since the tumor cannot be surgically removed in its mature stages, the chief cause of the rising death rate is late diagnosis of the disease. Additionally, HGSOC can only be effectively treated in its early stages with the targeted compound obtained after the results. One protein that is overexpressed in HGSOC was considered for this investigation, KLK7. According to recent research, the protein KLK7 is overexpressed in HGSOC and may be a practicable target for treatment to improve patient survival. Therapeutic suppression of this protein shows promise. One protein was chosen for this investigation because it was overexpressed in HGSOC and its downregulation improved survival outcomes[14]. Because it exhibited higher sequence convergence than other structures, the protein structure chosen for this investigation was found on PDB ID: 6Y4S. The Saves v6.0 tool was also used to authorize the structure. The target's PDB structure was attained, and 88 compounds that met ADMET necessities were chosen from the IMPPAT library to prepare the receptor for molecular docking. Because the IMPPAT library has a widespread variety of phytochemicals, it was used.

Table 3 and Table S1 list the ten substances with the lowest binding energy. Since compound 1 exhibits the lowest binding energy for KLK7, which is expressed in the primary tumor, it was selected for supplementary examination. Compound-1 has anti-cancer potential as well. Aristolactam-N-beta-D-glycoside, a phytochemical taken from IMPPAT, served as the study's reference chemical. Molecular docking with the receptors revealed that KLK7's binding energy was − 8.2 kcal/mol. Previous studies have mainly focused on synthetic KLK7 inhibitors like peptide-based compounds or coumarin derivatives, which often face challenges related to stability and selectivity[41]. In contrast, our findings suggest that Aristolactam-N-β-D-glycoside, a naturally occurring phytochemical, may offer a promising alternative with better binding potential and structural novelty.

The chemical with the highest affinity is the one with the lowest binding energy. To verify the ligands' kinetic stability and chemical reactivity, the complexes with the lowest binding energies underwent additional study using DFT. Compound-1 has an energy gap of 0.13272 eV. The chemical is reactive with our receptor KLK7, as designated by the smaller energy gap. The compound's reactivity was examined using DFT analysis, and the MD simulation offered additional confirmation. To verify the stability of the ligand–protein complex, compound 1 was used in an MD simulation of KLK7. MD simulations of KLK7 were carried out using compound-1 to confirm the stability of the ligand–protein complex. MD simulations were performed for 100 ns for the proteins. The largest RMSD value for KLK7 never exceeded 2 Å, suggesting that the protein–ligand combination remained stable throughout the run. Because the complex's radius of gyration was less than 30 Å and stayed constant for 100 ns, it is stable[42]. Only the initial fluctuation for KLK7 is the largest for the RMSF analysis, and no subsequent fluctuation for the complex above 3 Å, and no noticeable variations were observed in the complex's active site residues. Hydrogen bonds were created during MD simulation[32], indicating the complex's stability. The
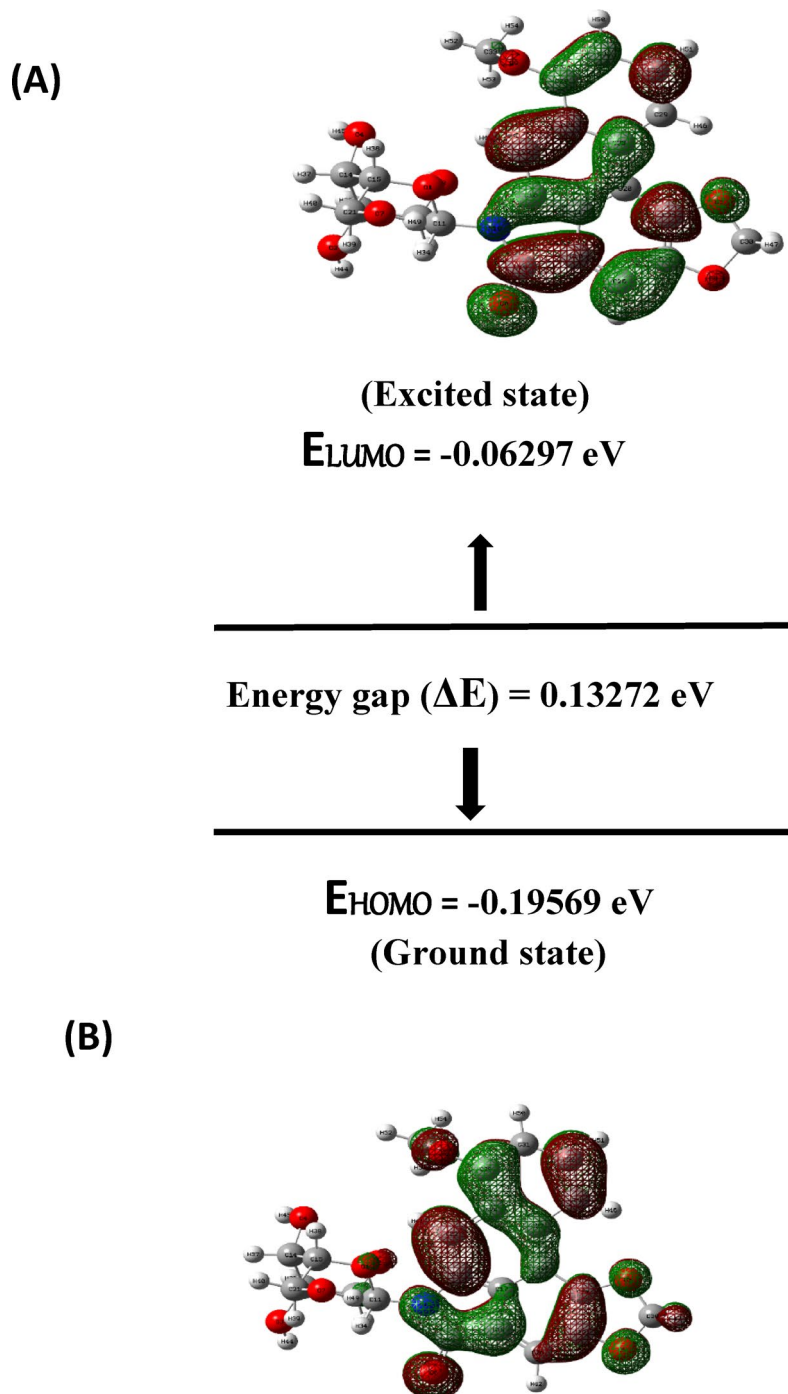
(A)

(Excited state)

$E_{LUMO} = -0.06297$ eV

Energy gap (ΔE) = 0.13272 eV

$E_{HOMO} = -0.19569$ eV
(Ground state)

(B)

Fig. 3. Compound-1's quantum description: ΔE is 0.13272 eV. Compound-1 is shown in the ground state (EHOMO) in (**B**) and in the excited state (ELUMO) in (**A**). (It was made using the Gauss View 6.0 software).

combination of KLK7 and Aristolactam-N-beta-D-glycoside showed stability with an RMSD[31] value fluctuating by roughly 2.8 Å.

Aristolochia plants, particularly Aristolochia indica, are the foundation of the natural alkaloid glycoside known as Aristolactam-N-β-D-glucoside (ADG)[43]. This constituent is a participant of the alkaloids' aristolochic acid group, which is known for its wide assortment of pharmacological features. ADG differs from other aristolochic acids due to the presence of the β-D-glucoside moiety, which also gives it special interactions with biomacromolecules[44]. Common ligand Aristolactam-N-beta-D-glycoside (compound-1) has demonstrated promise as a therapeutic KLK7 inhibitor. Members of the Aristolochiaceae family of phytochemicals, which also includes compounds derived from plants in the Aristolochia genus, include this chemical molecule, Aristolactam-N-beta-D-glycoside[45]. One substance that has been shown to have several biological roles is aristolactam-N-beta-D-glycoside[45]. Recent studies suggest that KLK7 contributes to tumor aggressiveness by breaking down the
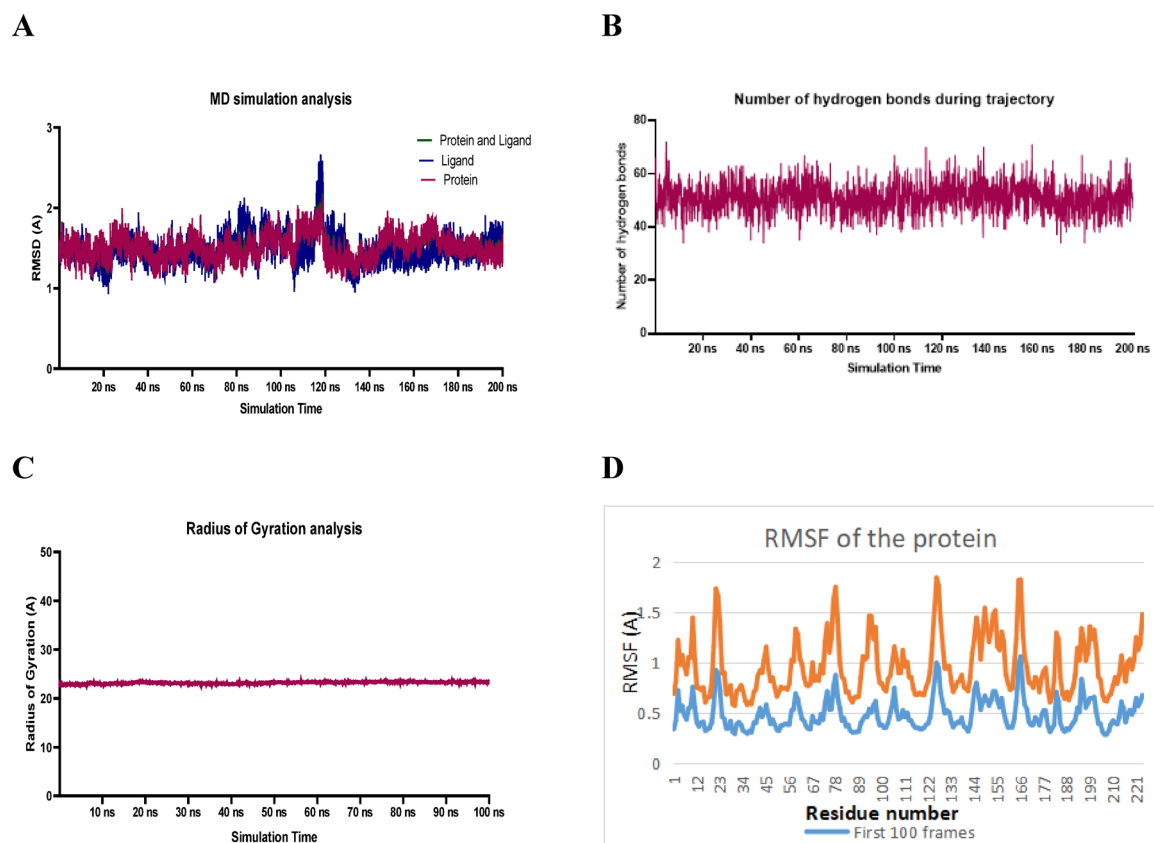
Fig. 4. MD simulation analysis of the KLK7 Aristolactam-N-beta-D-glycoside complex. (**A**) RMSD over 200 ns showing the stability of KLK7, Aristolactam-N-beta-D-glycoside complex, and Aristolactam-N-beta-D-glycoside alone. (**B**) Hydrogen bond count throughout the simulation, indicating interaction stability. (**C**) Radius of Gyration showing KLK7 compactness over time. (**D**) RMSF indicating residue flexibility, comparing the initial and final 1000 frames.

extracellular matrix, which can make it easier for cancer cells to detach and spread. Additionally, KLK7 appears to play a role in driving epithelial-to-mesenchymal transition (EMT), a key process that helps ovarian cancer cells invade surrounding tissues and resist treatment[15].

These include Anticancer: Studies have demonstrated the anticancer properties of aristolactams and their derivatives[43]. Anti-inflammatory: They may have anti-inflammatory properties, depending on their structure. Toxicity: Nephrotoxicity, or damage to the kidneys, and carcinogenicity are important factors to consider for some members of the aristolochic acid family, which includes aristolactams. Aristolactam-N-beta-D-glycoside is therefore regarded as an anti-KLK7 drug that aids in regulating KLK7 expression and has potential therapeutic uses. Before being employed as a possible treatment for patients with pancreatic cancer, additional experimental research would be required to confirm the in-silico consequences and evaluate the effectiveness and safety of the discovered inhibitors. But before they can be employed as possible treatments for HGSO cancer patients, more experimental research would be required to confirm the in-silico results and estimate the safety and effectiveness of the discovered inhibitors.

Conclusion

Computational analysis is a quick and proficient method for drug design because it doesn't require money and can rapidly identify a possible inhibitor. Data validated that KLK7, which is overexpressed in HGSOC, contributes to the disease's progression. To identify a possible inhibitor for this protein, which was chosen as a receptor, computational analysis was done. Compound-1 (PubChem ID: 159,819) was selected for an additional MD simulation examination of the protein because it unveiled the lowest binding energy with the protein expressed in the tumor KLK7. Our findings serve as a preliminary computational step, and in vitro/in vivo validation, along with toxicity screening, will be critical for assessing its drug-likeness and safety. All of these findings advocate that compound-1 may be a KLK7 inhibitor. The field of medication design and the management of HGSOC will be significantly impacted by this work. The results of this study establish how computational analysis can be used in drug design to create novel therapies for disorders like HGSOC. Some more detailed analyses, such as principal component analysis (PCA) and binding free energy estimations (MM-PBSA/MM-GBSA), are required for further studies. Moreover, in vitro assays such as surface plasmon resonance (SPR) or fluorescence-based binding studies, followed by cellular assays to evaluate biological activity and toxicity profiles. These steps would

be essential to verify computational predictions and assess the therapeutic potential in a more physiologically relevant context.

Data availability

References

1. Jemal, A. et al. Global cancer statistics. *CA: A Cancer J. Clin.* **61**(2), 69–90. https://doi.org/10.3322/caac.20107 (2011).
2. Ferlay, J. et al. Cancer incidence and mortality worldwide: Sources, methods and major patterns in GLOBOCAN 2012. *Int. J. Cancer* **136**(5), E359–E386. https://doi.org/10.1002/ijc.29210 (2015).
3. Kurman, R. J. & Shih, I.-M. The dualistic model of ovarian carcinogenesis. *Am. J. Pathol.* **186**(4), 733–747. https://doi.org/10.1016/j.ajpath.2015.11.011 (2016).
4. Lisio, M.-A., Fu, L., Goyeneche, A., Gao, Z. & Telleria, C. High-grade serous ovarian cancer: basic sciences, clinical and therapeutic standpoints. *Int. J. Mol. Sci.* **20**(4), 952. https://doi.org/10.3390/ijms20040952 (2019).
5. Mahmood, R. D., Morgan, R. D., Edmondson, R. J., Clamp, A. R. & Jayson, G. C. First-line management of advanced high-grade serous ovarian cancer. *Curr. Oncol. Rep.* **22**(6), 64. https://doi.org/10.1007/s11912-020-00933-8 (2020).
6. Zhu, Q. et al. Mechanism of LncRNA Gm2044 in germ cell development. *Front. Cell Develop. Biol.* **12**, 1410914. https://doi.org/10.3389/fcell.2024.1410914 (2024).
7. Zhou, J. et al. Network pharmacology combined with experimental verification to explore the potential mechanism of naringenin in the treatment of cervical cancer. *Sci. Rep.* **14**(1), 1860. https://doi.org/10.1038/s41598-024-52413-9 (2024).
8. Liu, P. et al. A pyroptosis-related LncRNA signature for predicting prognosis, immune features and drug sensitivity in ovarian cancer. *OncoTargets Ther.* **18**, 585–601. https://doi.org/10.2147/OTT.S491130 (2025).
9. Zhou, J. et al. Chrysotoxine regulates ferroptosis and the PI3K/AKT/mTOR pathway to prevent cervical cancer. *J. Ethnopharmacol.* **338**, 119126. https://doi.org/10.1016/j.jep.2024.119126 (2025).
10. Lin, Q. et al. A clinical prognostic model related to T cells based on machine learning for predicting the prognosis and immune response of ovarian cancer. *Heliyon* **10**(17), e36898. https://doi.org/10.1016/j.heliyon.2024.e36898 (2024).
11. Han, Q. et al. Built-in field-driven S-scheme boron-doped nanodiamond/TiO2(101)/MXene photocatalyst for efficient antibiotic elimination: mechanisms and DFT validation. *Chem. Eng. J.* **519**, 165290. https://doi.org/10.1016/j.cej.2025.165290 (2025).
12. Sun, W. et al. Tumor-targeting and redox-responsive photo-cross-linked nanogel derived from multifunctional hyaluronic acid-lipoic acid conjugates for enhanced in vivo protein delivery. *Int. J. Biol. Macromol.* **314**, 144444. https://doi.org/10.1016/j.ijbiomac.2025.144444 (2025).
13. Boyarskikh, U. A. et al. Spectrum of TP53 mutations in BRCA1/2 associated high-grade serous ovarian cancer. *Front. Oncol.* **10**, 1103. https://doi.org/10.3389/fonc.2020.01103 (2020).
14. Gong, W. et al. Prognostic value of kallikrein-related peptidase 7 (KLK7) mRNA expression in advanced high-grade serous ovarian cancer. *J. Ovarian Res.* **13**(1), 125. https://doi.org/10.1186/s13048-020-00725-5 (2020).
15. Riedel, M., Bronger, H., Magdolen, V. & Dreyer, T. The prognostic and diagnostic potential of kallikrein-related peptidases in ovarian cancer. *Expert Rev. Mol. Diagn.* **21**(6), 535–545. https://doi.org/10.1080/14737159.2021.1924680 (2021).
16. Farhani, I., Nezafat, N. & Mahmoodi, S. Designing a novel multi-epitope peptide vaccine against pathogenic *Shigella* spp. Based immunoinformatics approaches. *Int. J. Peptide Res. Ther.* **25**(2), 541–553. https://doi.org/10.1007/s10989-018-9698-5 (2019).
17. Laskowski, R. A., MacArthur, M. W., Moss, D. S. & Thornton, J. M. PROCHECK: a program to check the stereochemical quality of protein structures. *J. Appl. Crystallogr.* **26**(2), 283–291. https://doi.org/10.1107/S0021889892009944 (1993).
18. Eisenberg, D., Lüthy, R., & Bowie, J. U. [20] VERIFY3D: Assessment of protein models with three-dimensional profiles 396–404 (1997). https://doi.org/10.1016/S0076-6879(97)77022-8.
19. Bose-Brill, S. et al. A portfolio coach-informed professional development framework. *J. Contin. Educ. Heal. Prof.* **43**(4), 217–224. https://doi.org/10.1097/CEH.0000000000000502 (2023).
20. Binkowski, T. A. CASTp: Computed atlas of surface topography of proteins. *Nucleic Acids Res.* **31**(13), 3352–3355. https://doi.org/10.1093/nar/gkg512 (2003).
21. Jendele, L., Krivak, R., Skoda, P., Novotny, M. & Hoksza, D. PrankWeb: A web server for ligand binding site prediction and visualization. *Nucleic Acids Res.* **47**(W1), W345–W349. https://doi.org/10.1093/nar/gkz424 (2019).
22. Eberhardt, J., Santos-Martins, D., Tillack, A. F. & Forli, S. AutoDock Vina 1.2.0: New docking methods expanded force field and python bindings. *J. Chem. Inform. Model.* **61**(8), 3891–3898. https://doi.org/10.1021/acs.jcim.1c00203 (2021).
23. Benet, L. Z., Hosey, C. M., Ursu, O. & Oprea, T. I. BDDCS, the rule of 5 and drugability. *Adv. Drug Deliv. Rev.* **101**, 89–98. https://doi.org/10.1016/j.addr.2016.05.007 (2016).
24. Enna, S. J., Williams, M., Frechette, R., Kenakin, T., McGonigle, P., & Ruggeri, B. *Current Protocols in Pharmacology* (John Wiley & Sons, Inc, 2001). https://doi.org/10.1002/0471141755.
25. Trott, O. & Olson, A. J. AutoDock Vina: Improving the speed and accuracy of docking with a new scoring function, efficient optimization, and multithreading. *J. Comput. Chem.* **31**(2), 455–461. https://doi.org/10.1002/jcc.21334 (2010).
26. Bredas, J.-L. Mind the gap!. *Mater. Horiz.* **1**(1), 17–19. https://doi.org/10.1039/C3MH00098B (2014).
27. Phillips, J. C. et al. Scalable molecular dynamics on CPU and GPU architectures with NAMD. *J. Chem. Phys* https://doi.org/10.1063/5.0014475 (2020).
28. Humphrey, W., Dalke, A. & Schulten, K. VMD: Visual molecular dynamics. *J. Mol. Graph.* **14**(1), 33–38. https://doi.org/10.1016/0263-7855(96)00018-5 (1996).
29. Colovos, C. & Yeates, T. O. Verification of protein structures: Patterns of nonbonded atomic interactions. *Protein Sci.* **2**(9), 1511–1519. https://doi.org/10.1002/pro.5560020916 (1993).
30. Lüthy, R., Bowie, J. U. & Eisenberg, D. Assessment of protein models with three-dimensional profiles. *Nature* **356**(6364), 83–85. https://doi.org/10.1038/356083a0 (1992).
31. Martínez, L. Automatic identification of mobile and rigid substructures in molecular dynamics simulations and fractional structural fluctuation analysis. *PLoS ONE* **10**(3), e0119264. https://doi.org/10.1371/journal.pone.0119264 (2015).
32. Lobanov, MYu., Bogatyreva, N. S. & Galzitskaya, O. V. Radius of gyration as an indicator of protein structure compactness. *Mol. Biol.* **42**(4), 623–628. https://doi.org/10.1134/S0026893308040195 (2008).
33. Prat, J., D'Angelo, E. & Espinosa, I. Ovarian carcinomas: At least five different diseases with distinct histological features and molecular genetics. *Hum. Pathol.* **80**, 11–27. https://doi.org/10.1016/j.humpath.2018.06.018 (2018).
34. Shabir, S. & Gill, P. K. Global scenario on ovarian cancer—Its dynamics, relative survival, treatment, and epidemiology. *Adesh Univ. J. Med. Sci. Res.* **2**, 17. https://doi.org/10.25259/AUJMSR_16_2019 (2020).

35. Punzón-Jiménez, P., Lago, V., Domingo, S., Simón, C. & Mas, A. Molecular management of high-grade serous ovarian carcinoma. *Int. J. Mol. Sci.* **23**(22), 13777. https://doi.org/10.3390/ijms232213777 (2022).
36. Azzalini, E., Stanta, G., Canzonieri, V. & Bonin, S. Overview of tumor heterogeneity in high-grade serous ovarian cancers. *Int. J. Mol. Sci.* **24**(20), 15077. https://doi.org/10.3390/ijms242015077 (2023).
37. Kandalaft, L. E., Dangaj Laniti, D. & Coukos, G. Immunobiology of high-grade serous ovarian cancer: Lessons for clinical translation. *Nat. Rev. Cancer* **22**(11), 640–656. https://doi.org/10.1038/s41568-022-00503-z (2022).
38. Javellana, M., Hoppenot, C. & Lengyel, E. The road to long-term survival: Surgical approach and longitudinal treatments of long-term survivors of advanced-stage serous ovarian cancer. *Gynecol. Oncol.* **152**(2), 228–234. https://doi.org/10.1016/j.ygyno.2018.11.007 (2019).
39. Chowdhury, S. et al. Proteogenomic analysis of chemo-refractory high-grade serous ovarian cancer. *Cell* **186**(16), 3476-3498.e35. https://doi.org/10.1016/j.cell.2023.07.004 (2023).
40. Haider, F. et al. Investigation of phytoestrogens found in sesame seeds via computational and translational approaches. *BioScientific Rev.* **5**(4), 53–68. https://doi.org/10.32350/BSR.54.05 (2023).
41. Molehin, D., Yamasaki, K. & Nakatsuji, T. Structure and function of kallikrein-related peptidases: Implications for skin diseases and therapeutic targeting. *Front. Immunol.* **11**, 581213. https://doi.org/10.3389/fimmu.2020.581213 (2020).
42. Mateen, R. M. et al. Drug repurposing: Identification of potential drug targets against nonstructural protein 1 (NSP-1) of SARS-CoV-2 through molecular docking and molecular dynamic simulation using FDA approved drugs. *J. Microbiol. Mol. Genet.* **3**(3), 161–178 (2022).
43. Ray, A., Kumar, G. S. & Maiti, M. Molecular aspects on the interaction of aristololactam-β-D-glucoside with H ^{L} -form deoxyribonucleic acid Structures. *J. Biomol. Struct. Dyn.* **21**(1), 141–151. https://doi.org/10.1080/07391102.2003.10506912 (2003).
44. Marti, G. et al. Natural aristolactams and aporphine alkaloids as inhibitors of CDK1/Cyclin B and DYRK1A. *Molecules* **18**(3), 3018–3027. https://doi.org/10.3390/molecules18033018 (2013).
45. Das, A. & Kumar, G. S. Natural Aristolochia alkaloid Aristololactam-β-D-glucoside: Interaction with biomacromolecules and correlation to the biological perspectives. *Mini-Rev. Med. Chem.* **18**(12), 1022–1034. https://doi.org/10.2174/1389557518666180222170050 (2018).

Acknowledgements

Author contributions

The manuscript was written with the contributions of all authors. All authors have approved the final version of the manuscript.

Funding

Declarations

Competing interests

The authors declare no competing interests.

Additional information

Supplementary Information The online version contains supplementary material available at https://doi.org/10.1038/s41598-025-18364-5.

Correspondence and requests for materials should be addressed to A.B. or S.I.

Reprints and permissions information is available at www.nature.com/reprints.

Publisher's note Springer Nature remains neutral with regard to jurisdictional claims in published maps and institutional affiliations.